Korean J. Chem. Eng., 38(2), 400-405 (2021)
DOI: 10.1007/s11814-020-0703-2

pISSN: 0256-1115
eISSN: 1975-7220

Theoretical investigation on the throttle pressure reducing valve through CFD simulation and validating experiments

Enle Xu*,, Chenglei Nie***, Xiaofeng Jiang*, and Zhenyong Miao*,†**

*School of Chemical Engineering and Technology, China University of Mining and Technology, Xuzhou, Jiangsu 221116, China
**College of Electromechanical Engineering, Qingdao University of Science and Technology, Qingdao, Shandong, 266061, China
***State Key Laboratory of Nuclear Power Safety Monitoring Technology and Equipment, China Nuclear Power Engineering Co. Ltd., Shenzhen, Guangdong, 518172, China
(*Received 14 August 2020 • Revised 14 October 2020 • Accepted 28 October 2020*)

Abstract−The throttle pressure reducing valve has potential for the high pressure heat exchanger with the advantage of simple structure, easy operation and maintenance. We investigated the discharge capacity under different pressure difference between inlet and outlet, the area of inlet and throttle though CFD simulation and validating experiments. A theoretical formula of the discharge capacity was developed through the theoretical analysis and simulated results and was well proved by the experiments. The results revealed that the square of discharge capacity is positively proportional to the pressure difference, and the drag coefficient has a linear relationship with the throttle area and the reciprocal of flange area. This research establishes the theoretical basis for the designing and engineering application of throttle pressure reducing valve.

Keywords: Throttle, Pressure Reducing Valve, High Pressure Heat Exchanger, Trap Valve

INTRODUCTION

The high pressure heat exchanger (HPHE) is one of key devices for improving the thermal efficiency in a modern thermal or nuclear power plant [1-4]. HPHE transfers the energy of high pressure steam from steam turbine to the feedwater in order to increase its temperature. When high pressure steam is lower than the saturation temperature, the steam will turn into water stored at the bottom of HPHE. The height of water level in HPHE is a key parameter in performance of keeping heaters operating safely and economically [5]. If the water level is too high, the effective heat transfer area will be less and the economy of this device will be reduced. In severe cases, the high water level will damage the heat exchanger, so the heat exchanger runs in the low water level for security. However, high pressure steam will escape from HPHE under the low or no water level height, a condition which is uneconomic and should be avoided. Thus, it is necessary to ensure the water level in a reasonable range for HPHE utilizing a trap valve [6,7]. In general, condensate water will flow into next stage heat exchanger with lower pressure than HPHE in order to recover the condensate water heat of HPHE. The product of condensate water is almost unchanged during normal operation in HPHE. So, the discharge capacity needs to keep stable under the environment of high pressure difference for the trap valve called as pressure-reducing valve (PRV).

Numerous studies have investigated different structure PRV used in HPHE and simulated its internal flow characteristics. Jin et al. [8] developed a new PRV combining a forge-welded angle-type single seat plug with a double throttling structure. Luo and He et al. [9,10] developed a PRV with a constant pressure ratio and analyzed the pressure and leakage characteristics of the valve in a water hydraulic vane pump. Jin et al. [11] proposed a novel high multi-stage PRV. The inner and outer porous shrouded valve core and porous orifice plate are chosen as the first-stage and second-stage throttling component, respectively. Qian et al. [12] investigated the Mach number and proposed the design method in multi-stage perforated plates in high PRV. Wei et al. [13,14] studied the characteristics of flow-induced noise in high PRV based on computational fluid dynamics. Hou et al. [15] did a parametric study of internal flow and throttling characteristics in a multi-stage high PRV with turbulent model.

Meanwhile, other kinds of valves used at the condition of high pressure difference was investigated. Saha et al. [16] designed a pressure regulating and shut-off valve to reduce high inlet pressure to a lower level of outlet pressure which remains almost constant. Beune et al. [17,18] analyzed the opening characteristic and given insight into the valve dynamics of an opening safety valve by the method of fluid-structure interaction. Qian et al. [19] simulated the dynamic characteristics of pilot-control globe valve which utilizes the pressure difference before and after the valve to control the action of the valve core. Zhang et al. [20] proposed a self-operated three-way valve driven by the pressure difference between the inlet and outlet used in a hybrid air conditioner. Chalet et al. [21] developed a new throttle valve model considering the flow characteristics and geometrical parameters and determined the engine performance

†To whom correspondence should be addressed.
E-mail: zymiao@cumt.edu.cn
Copyright by The Korean Institute of Chemical Engineers.

at partial load.

Based on the foregoing description, an ample variety of PRV was investigated; however, few researchers have focused on the throttle PRV. Due to the simple structure, easy operation and maintenance, the throttle PRV would be widely used in the system of HPHE. However, the specific relationship or function among the discharge capacity of the throttle PRV, pressure difference and structure parameters still requires further analysis and clarification.

In this paper, numerical simulation and validating experiments were implemented to reveal how the pressure difference and structural parameters influence the discharge capacity of the throttle PRV and establish a theoretical formula to predict the discharge capacity under different working conditions.

DESCRIPTION OF THE THROTTLE PRV

1. Throttle PRV Structure

A schematic representation of the throttle PRV is provided in Fig. 1. The key components of the throttle PRV are two flanges and a throttle. The throttle is fixed by the flanges through some bolts and a sealing gasket prevents water leakage. The area difference between the flange and throttle determines the discharge capacity. The throttle results in the pressure reducing due to the damping effect.

2. Theoretical Analysis of Throttle PRV

The pressure difference provided in Eq. (1) can be calculated according to Bernoulli equation when the liquid flows through the throttle.

$$\Delta p = \frac{\delta \rho u^2}{2} \tag{1}$$

where Δp is pressure difference between inlet and outlet, Pa; u is the throttle velocity descripted in Eq. (2), m/s; ρ is the liquid density, kg/m^3; δ is drag coefficient which has relation with the area of throttle and flange showed in Eq. (3).

$$u = \frac{Q}{A_0} \tag{2}$$

where Q is volume discharge capacity, m^3/s; A_0 is the throttle area, m^2.

$$\delta = f\left(\frac{A_0}{A_1}\right) \tag{3}$$

where A_1 is the flange area, m^2; f represents an uncertain function which would be confirmed based on the next simulated results.

According to Eqs. (1)-(3), Q can be redescribed as

$$Q^2 = \frac{2\Delta p A_0^2}{\rho f\left(\frac{A_0}{A_1}\right)} \tag{4}$$

The relation among Q, Δp A_0 and A_1 would be validated by means of computational fluid dynamic simulation and validated experiments in the next part.

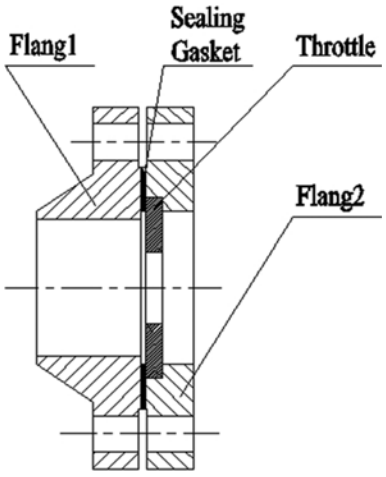

Fig. 1. The schematic representation of the throttle PRV.

THEORETICAL AND NUMERICAL METHODOLOGIES

1. Computational Model

A three-dimensional geometrical model was built in the preprocessor ANSYS Workbench Design Modeler based on the structure in Fig. 1. Fig. 2(a) shows the mesh model produced in the software of ICEM 14.5. The cross-sectional view of the outlet is provided in Fig. 2(b). In this figure, the throttle and flange diameter is 8 mm and 32 mm. The area of inlet flange is the same with that of outlet flange. The lengths of inlet flange, throttle and outlet flange are 15 mm, 6 mm, 100 mm, respectively. The O-grid block is chosen as grid topology to produce the structured mesh. The mesh size of throttle and flange is about 0.75 mm. Orthogonal quality was used to analyze the quality of the meshes. The minimum orthogonal quality was 0.73, which stated that the grids is nice to be computed in the simulation.

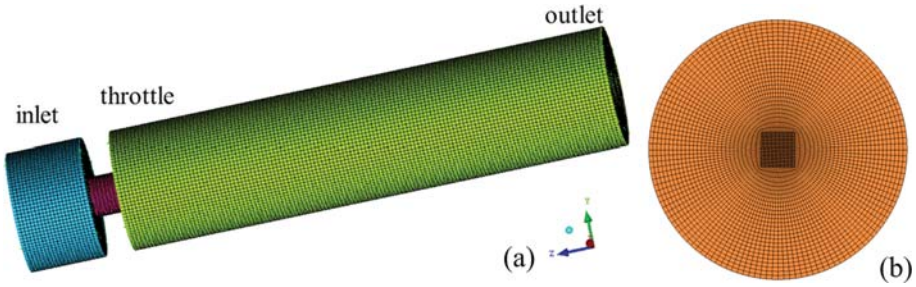

Fig. 2. (a) Computational mesh of throttle PRV (b) cross-sectional view of outlet.

2. Governing Equations

The continuity equation based on the incompressible fluid could be described as

$$\nabla \cdot \vec{v} = 0 \tag{5}$$

The momentum equation is expressed as

$$\nabla \cdot (\rho \vec{v}\vec{v}) = -\nabla p + \nabla \cdot [\mu(\nabla \vec{v} + (\nabla \vec{v})^T)] + \rho g \tag{6}$$

where ρ is the fluid density, kg/m^3; $\vec{v}$ is the velocity vector, m/s; p is the static pressure force, N; μ is the molecular viscosity, Pa·s; ρg is the gravitational body force, N [22,23].

The turbulent viscosity, μ_t, is calculated by the standard k-ε model where k is the turbulent kinetic energy and ε is the dissipation rate.

$$\mu_t = \frac{c_\mu \rho k^2}{\varepsilon} \tag{7}$$

The turbulent kinetic energy equation simplifies to

$$\frac{\partial(\rho k u_i)}{\partial x_i} = \frac{\partial}{\partial x_j}\left[\left(\mu + \frac{\mu_t}{\sigma_k}\right)\frac{\partial k}{\partial x_j}\right] + G_k - \rho\varepsilon \tag{8}$$

The turbulent dissipation ratio equation simplifies to

$$\frac{\partial(\rho \varepsilon u_i)}{\partial x_i} = \frac{\partial}{\partial x_j}\left[\left(\mu + \frac{\mu_t}{\sigma_\varepsilon}\right)\frac{\partial \varepsilon}{\partial x_j}\right] + \frac{c_1 \varepsilon}{k} - c_2 \rho \frac{\varepsilon^2}{k} \tag{9}$$

where u_i is the time averaged velocity, m/s; G_k represents the generation of turbulence kinetic energy due to the mean velocity gradients, m^2/s^2. The constants c_1, c_2, c_μ, σ_k, and σ_ε are 1.44, 1.92, 0.09, 1.0 and 1.3, respectively [24].

3. Simulation Scheme

Governing Eqs. (5)-(9) were solved in the software of Fluent 14.5. The pressure-based solver was chosen to solve the governing equations. The SIMPLE scheme and least squares cell based of gradient were employed in the calculation process. The standard scheme was taken for pressure term. The second-order upwind scheme was used for the momentum equations and the first-order upwind scheme was used for the turbulent kinetic energy and turbulent dissipation rate.

Water-liquid was chosen as the simulated material, with density 998.2 kg/m^3, and viscosity 0.001003 kg/(m·s). The boundary conditions for the inlet and outlet are pressure-inlet and pressure-outlet, respectively. The outlet pressure is fixed to zero. The inlet pressure is 0.50 MPa, 0.75 MPa, 1.0 MPa, 1.25 MPa, and 1.50 MPa, which changes with different simulation conditions. Residuals for governing equations are performed within 1.0×10^{-4} relative error as a criterion for convergence of the solution. Flow rate of inlet and outlet reaches a balanced and stable level, which is regarded as another convergence condition.

4. Mesh Independence

It is necessary to check the mesh independence before starting the simulation in order to eliminate the numerical errors. In this study, the mesh independence is based on applying different mesh numbers [25]. Through adjusting the mesh size, the different mesh number could be obtained. The simulated results of mass flow rate under different mesh numbers were compared in Fig. 3. As the mesh number increases, mass flow rate decreases first, and then remains stable. The reason may be that too large mesh size cannot detect the relevant flow features [26]. When mesh number increases from 733,069 to 904,808, the mass flow rate increases from 1.63 kg/s to 1.64 kg/s (0.6%). This finding indicates that enhancing the mesh number does not have an effect on the accuracy of the results [27,28]. However, considering the calculation time, the model with 733,069 mesh number was chosen for numerical simulation.

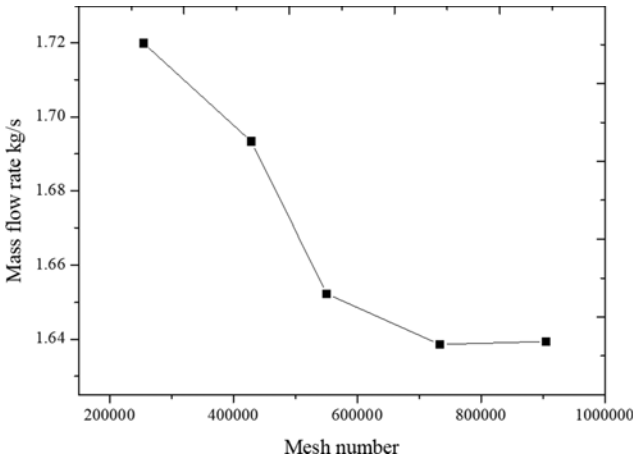

Fig. 3. Relation between the mass flow rate and mesh number.

RESULTS AND DISCUSSION

1. Relation between Q and Δp

Fig. 4 shows the pressure contour and velocity streamline of the central surface under different Δp of 0.5 MPa, 1.0 MPa and 1.5

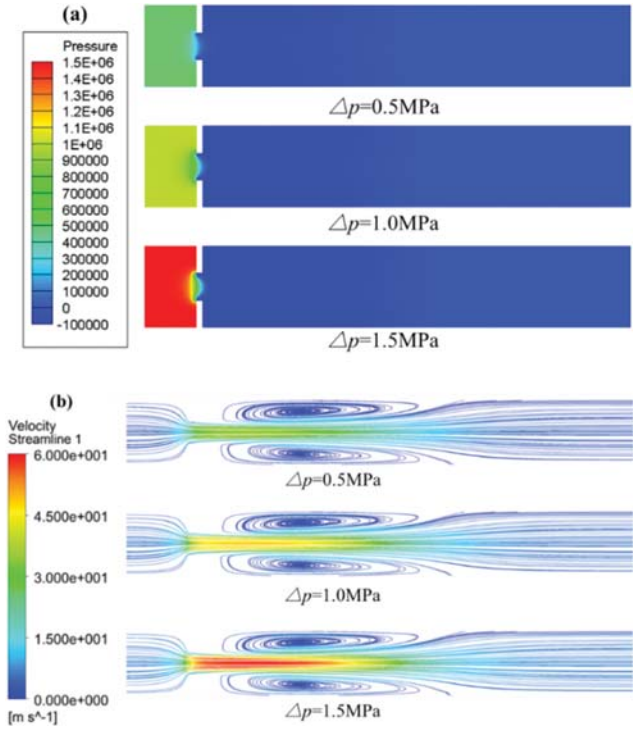

Fig. 4. (a) pressure contour and (b) velocity streamline under different Δp of 0.5 MPa, 1.0 MPa and 1.5 MPa.

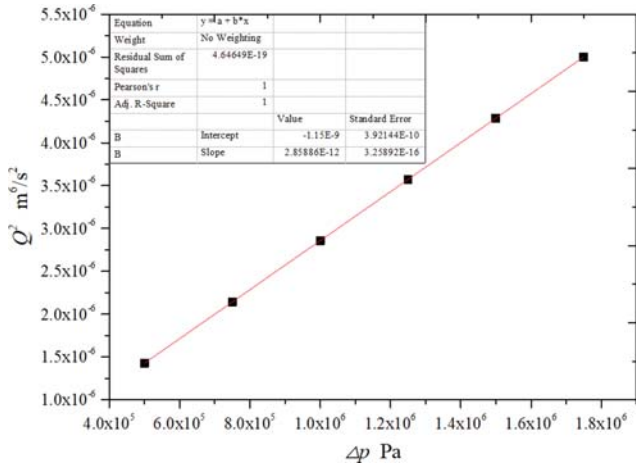

Fig. 5. Relation between Δp and Q^2.

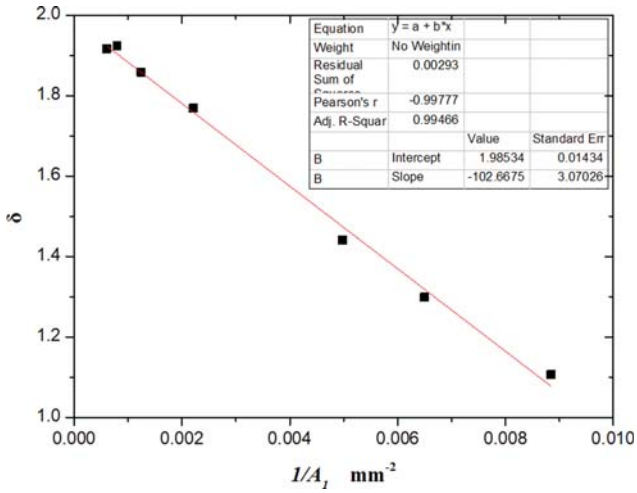

Fig. 6. Relation between δ and $1/A_1$.

MPa. From these pressure contours, the pressure difference occurs in the location of before and after of the throttle. It can be concluded that the area difference between flange and throttle is one main reason to cause the pressure difference. According to velocity streamline, the throttle velocity increases with the increasing of Δp, which will lead to raising of the discharge capacity. In turn, the larger throttle velocity will also lead to more fluid resistance. In addition, a vortex will form behind the throttle for the reason that the high speed fluid through the throttle could not spread completely the pipeline immediately, which is another reason for the pressure difference. As a consequence, the discharge capacity presents the tendency of nonlinear increase with the increment of Δp.

The relation between Δp and Q^2 is shown in Fig. 5. The volume flow rate Q increases with the increase of Δp, which has been explained based on the Fig. 4(b). According to the fitting equation, Q^2 is a linear function with Δp and the very small intercept can be ignored, which is identical with Eq. (4), indicating that the theoretical equation is reasonable. Combined with Eq. (4) and Fig. 5, it can be concluded that the pressure difference has no impact on the drag coefficient, δ.

2. Relation between δ and A_1

For the purpose of obtaining the relation between δ and A_1, the models with different A_1 and unchanged A_0 and Δp were simulated. The unchanged diameter of A_0 is 8 mm, Δp is 1.0 MPa, and the difference diameter of A_1 is 12 mm, 14 mm, 16 mm, 24 mm, 32 mm, and 40 mm, respectively. The δ could be calculated on the basis of Eq. (1) where Δp and Q obtained from simulated results. Fig. 6 provides the relation between δ and $1/A_1$. Under the same Δp and A_0, the bigger A_1 will reduce discharge capacity and enlarge δ, so the δ decreases with the increasing of $1/A_1$. According to the fitting equation in Fig. 6, it is a linear relationship between δ and $1/A_1$, which can be expressed as Eq. (10).

$$\delta = \frac{k_1}{A_1} + b_1 \tag{10}$$

3. Relation between δ and A_0

To investigate the relation between δ and A_0, the models with different A_0 and unchanged A_1 and Δp were simulated. The unchanged diameter of A_1 is 24 mm, Δp is 1.0 MPa, and the different diameter of A_0 is 4.8 mm, 6.0 mm, 8.0 mm, 12 mm, 15 mm, and 18 mm, respectively. Fig. 7 provides the relation between δ and A_0. Under the same Δp and A_1, the bigger A_0 will allow more liquid through the throttle, then magnify discharge capacity and shrink δ. Thus, the δ decrease with the increasing of A_0. According to the fitting equation in Fig. 7, the δ is inversely proportional to A_0, which can be described as Eq. (11).

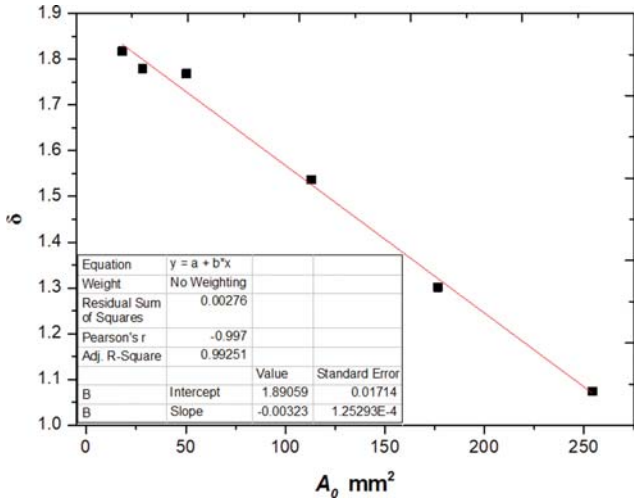

Fig. 7. Relation between δ and A_0.

$$\delta = k_2 A_0 + b_2 \tag{11}$$

4. Relation between δ and A_0/A_1

Based on Eqs. (3), (10) and (11), the relation among δ, A_1 and A_0 can be re-described as

$$\delta = k\frac{A_0}{A_1} + b \tag{12}$$

The relation between δ and A_0/A_1 is shown in Fig. 8 which contains all the data in Fig. 6 and 7. From Fig. 8, it can be seen that the δ decreases with the increasing of A_0/A_1 and is in a linear func-

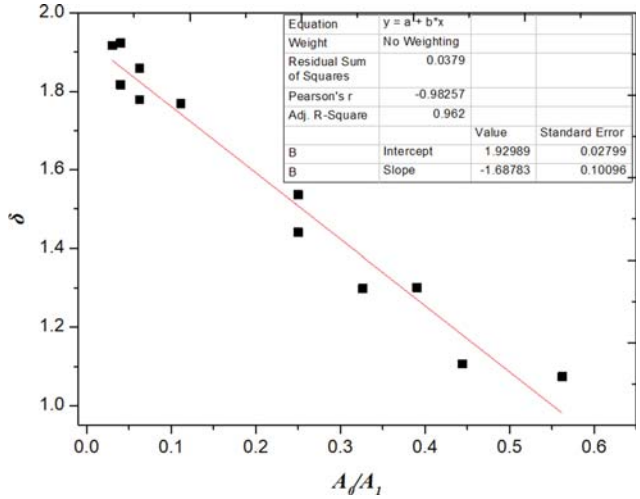

Fig. 8. Relation between δ and A_0/A_1.

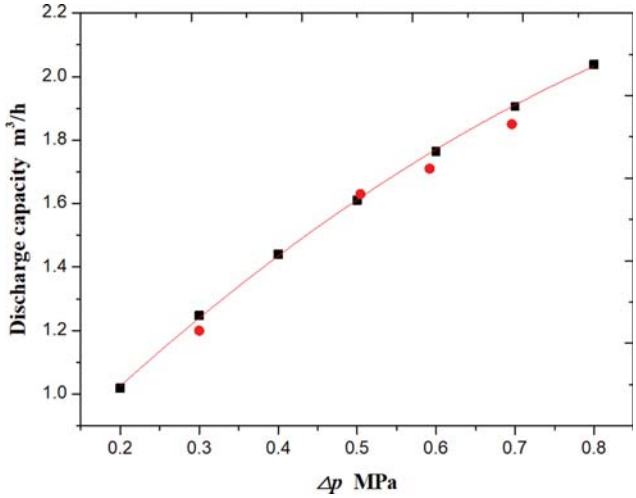

Fig. 10. Relation between discharge capacity and Δp.

tion with A_0/A_1 which matches with Eq. (12). According to the fitting equation in Fig. 8, Eq. (4) can be reorganized as Eq. (13).

$$Q^2=\frac{2\Delta p A_0^2 A_1}{\rho(-1.69A_0+1.93A_1)} \quad (13)$$

EXPERIMENT

1. Experimental System

To verify the simulated model, especially the theoretical Eq. (13), an experimental system was developed to test the performance of throttle PRV. Fig. 9 shows the experimental flow diagram. This system consists of a water tank, a high pressure pump, a bypass valve, a high pressure tank, a throttle PRV, a pressure transducer and a flow transducer. The high pressure pump was used to maintain the high pressure environment of this system. The high pressure tank was utilized to ensure a stable flow rate through the throttle PRV. The discharge capacity and pressure difference was adjusted by bypass valve nearby high pressure pump. The pressure and discharge capacity could be measured by the related transducers with a precision of ±0.5%.

In the experimental process, water as the working fluid flowed out the throttle PRV into the atmosphere, so the gauge pressure of outlet was zero. At the beginning of the experiment, the bypass valve should be full open. Then, the bypass valve was closed slowly until the pressure of high pressure tank reached 0.50 MPa, 0.75 MPa, 1.0 MPa, 1.25 MPa, and 1.50 MPa. Finally, the discharge capacity through the throttle PRV was obtained through the flow transducer when the flow rate reached a stable status.

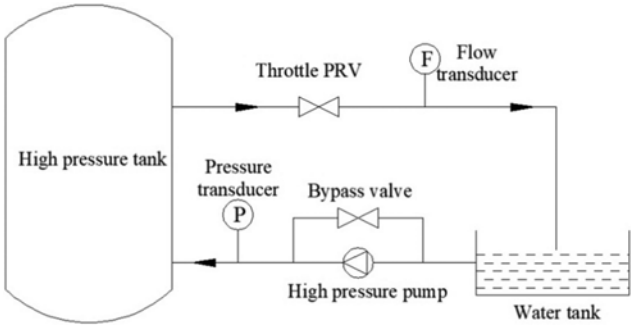

Fig. 9. Experimental flow diagram.

2. Experiment Validation

The discharge capacity was obtained under different Δp with A_1 diameter of 80 mm and A_0 diameter of 5 mm. The simulated and experimental results between discharge capacity and Δp are given in Fig. 10. In Fig. 10, the square points denote the theoretical results calculated on the basis of Eq. (13), and the circular points represent the experimental results. From Fig. 10, it can be seen that experimental discharge capacity increases with the increasing of Δp, which is in a good agreement with the simulated results, illustrating that the simulated model and the theoretical Eq. (13) are reliable.

CONCLUSION

The throttle PRV is widely used in the HPHE with the advantage of simple structure, easy operation and maintenance. To calculate the discharge capacity, the relations among discharge capacity, pressure difference between inlet and outlet, the area of inlet and throttle were investigated by means of CFD simulation and validating experiments. Based on the simulated results, the square of discharge capacity is positively proportional to pressure difference, and the drag coefficient has a linear relationship with the throttle area as well as the reciprocal of flange area. A theoretical formula of the discharge capacity was developed through theoretical analysis and proved by the experimental results.

This paper establishes the theoretical basis for the designing and engineering applications of throttle PRV. The theoretical formula introduces a simple way to calculate the discharge capacity under different operational condition and throttle structures.

ACKNOWLEDGEMENTS

This research was supported by China Postdoctoral Science

Foundation (2020M671654), Natural Science Foundation of Jiangsu Province (BK20190633), A Project of Shandong Province Higher Educational Science and Technology Program (J17KA181), the National Natural Science Foundation of China (51774285).

REFERENCES

1. M. Álvarez-Fernández, L. d. Portillo-Valdés and C. Alonso-Tristán, *Appl. Therm. Eng.*, **68**, 45 (2014).
2. G. Heo and S. K. Lee, *Expert Syst. Appl.*, **39**, 5078 (2012).
3. J. Xu, T. Yang, Y. Sun, K. Zhou and Y. Shi, *Appl. Therm. Eng.*, **67**, 179 (2014).
4. D. M. Godino, S. F. Corzo, N. M. Nigro and D. E. Ramajo, *Nucl. Eng. Des.*, **335**, 265 (2018).
5. S. Kim, B.-U. Bae, Y.-J. Cho, Y.-S. Park, K.-H. Kang and B.-J. Yun, *Nucl. Eng. Des.*, **260**, 54 (2013).
6. M. Gong, M. Peng and H. Zhu, *Appl. Therm. Eng.*, **140**, 190 (2018).
7. S. M. Hossienalipour, S. Karbalaee M and H. Fathiannasab, *Appl. Therm. Eng.*, **110**, 590 (2017).
8. Z. Jin, L. Wei, L. Chen, J. Qian and M. Zhang, *J. Zhejiang Univ-SCI A*, **14**, 137 (2013).
9. L. Luo, X. He, B. Den and X. Huang, *J. Press. Vessel Technol.*, **136**, 0216011 (2014).
10. X. He, B. Deng, X. Huang and X. Yan, *Adv. Mater. Res.*, **842**, 569 (2014).
11. Z. Jin, F. Chen, J. Qian, M. Zhang, L. Chen, F. Wang and Y. Fei, *Int. J. Hydrogen Energy*, **41**, 5559 (2016).
12. J. Qian, M. Zhang, L. Lei, F. Chen, L. Chen, L. Wei and Z. Jin, *Energy Convers. Manage.*, **119**, 81 (2016).
13. L. Wei and Z. Jin, *J. Acoust. Soc. Am.*, **134**, 4191 (2013).
14. Z. Jin, L. Wei, G. Zhu, J. Qian, Y. Fei and Z. Jin, *PLos One*, **10**, 01 (2015).
15. C. Hou, J. Qian, F. Chen, W. Jiang and Z. Jin, *Appl. Therm. Eng.*, **128**, 1238 (2018).
16. B. Saha, H. Chattopadhyay, P. Mandal and T. Gangopadhyay, *Comput. Fluids*, **101**, 233 (2014).
17. A. Beune, J. G. M. Kuerten and J. Schmidt, *AIChE J.*, **57**, 3285 (2011).
18. A. Beune, J. G. M. Kuerten and M. P. C. van Heumen, *Comput. Fluids*, **64**, 108 (2012).
19. J. Qian, L. Wei, Z. Jin, J. Wang, H. Zhang and A. Lu, *Energy Convers. Manage.*, **87**, 220 (2014).
20. P. Zhang, D. Zhou, W. Shi, X. Li and B. Wang, *Appl. Therm. Eng.*, **65**, 384 (2014).
21. D. Chalet and P. Chesse, *Eng. Appl. Comp. Fluid Mech.*, **4**, 387 (2010).
22. P. Feng, D. Chen, Y. Cao and Y. Chen, *Korean J. Chem. Eng.*, **37**, 604 (2020).
23. P. Zahedi, R. Saleh, R. Moreno-Atanasio and K. Yousefi, *Korean J. Chem. Eng.*, **31**, 1349 (2014).
24. L. Li and B. Xu, *Korean J. Chem. Eng.*, **33**, 2007 (2016).
25. S. E. Rafiee and M. M. Sadeghiazad, *Aerosp. Sci. Technol.*, **63**, 110 (2017).
26. J. Wackers, G. Deng, E. Guilmineau, A. Leroyer, P. Queutey, M. Visonneau, A. Palmieri and A. Liverani, *J. Comput. Phys.*, **344**, 364 (2017).
27. Y. Sun, J. Yu, W. Wang, S. Yang, X. Hu and J. Feng, *Korean J. Chem. Eng.*, **37**, 743 (2020).
28. S. E. Rafiee and M. M. Sadeghiazad, *J. Marine Sci. Appl.*, **15**, 388 (2016).